# *MASS TRANSFER ANALYSIS OF $CO_2$ CAPTURE BY PVDF MEMBRANE CONTACTOR AND IONIC LIQUID*

*Lucia Gómez-Coma*, Aurora Garea, Angel Irabien*

*Universidad de Cantabria, Departamento de Ingenierías Química y Biomolecular, E.T.S. de Ingenieros Industriales y Telecomunicación, Universidad de Cantabria, Avda Los Castros s/n 39005 Santander, Spain*

*Corresponding author: Tel: +34 942 206777, Fax: +34 942 201591

email: gomezcomal@unican.es

*This article contributes to carbon capture absorption studies strongly in order to advance in the intensified process. A novel technique using a PVDF hollow fibre membrane contactor and [emim][Ac] ionic liquid as absorbent has been performed. Competitive results compared with traditional absorption towers have been accomplished. Moreover, a theoretical simulation has been achieved in order to give the bases for scaling.*

*Abstract*

Post-combustion processes based on ionic liquids and membrane contactors have emerged as new attractive alternatives to traditional systems. In this work, a gas stream composed of 15% $CO_2$ and 85% $N_2$ flowed through the lumen side of a hollow fibre membrane contactor containing PVDF-IL fibres. An ionic liquid, 1-ethyl-3-methylimidazolium acetate [emim][Ac], was used as an absorbent due to its high chemical absorption and high $CO_2$ solubility. The overall mass transfer coefficient, activation energy, and resistances of the hollow fibre membrane were quantified from 303 to 343 K. The $K_{overall}$ value was one order of magnitude higher than those reported in previous works using conventional solvents, and the Ea was lower than previously reported values for other solvents.

A theoretical simulation was conducted to estimate the operational parameters required for 90% $CO_2$ capture and to quantify intensification effects related to $CO_2$ absorption in a packed column.

*Keywords*

*$CO_2$ capture, PVDF membrane contactors, [emim][Ac] ionic liquid, mass transfer coefficient.*

## *1. Introduction*

Since the beginning of the industrial revolution, the demand for energy has dramatically increased and has typically been met by burning fossil fuels [1, 2]. The combustion of fossil fuels produces carbon dioxide gas, which should be removed from industrial flue gas streams to mitigate environmental effects [3]. The emissions of carbon dioxide the atmosphere need therefore to be drastically reduced in order to alleviate the proven effects of global warming [4]. $CO_2$ concentration in the atmosphere has increased by more than 100 ppm since their pre-industrial levels (280 ppm), reaching 384 ppm in 2007 and nowadays this value is around 400ppm [5]. This value implies that during this period, the $CO_2$ abundance in the atmosphere increased substantially: the average rate of increase in $CO_2$ determined by direct instrumental measurements over the period 1960 to 2005 is 1.4 ppm per year [6]. The reduction of greenhouse gas concentrations in the atmosphere, especially $CO_2$, has been a significant goal of the 21$^{st}$ century. The capture and reuse of $CO_2$ is typically referred to as carbon capture and utilization (CCU). Current CCU technologies and processes are at different stages of maturity. In general, technical and economical improvements are needed to make CCU competitive. The cost of synthesizing $CO_2$-based products is highly dependent on the cost or value associated with a $CO_2$ unit. Therefore, the processing of $CO_2$ into other valuable products to mitigate climate change requires the optimization of $CO_2$ capture systems. Roussanaly et al., (2016) reported that Carbon Capture and Storage (CCS) is regarded as one of the most promising technologies for reducing man-made carbon atmospheric emissions, and is projected to provide 14% of the reduction in manmade greenhouse gas (GHG) emissions by 2050 [7].Three primary carbon dioxide capture methods are known: pre-combustion where $CO_2$ capture from gasified coal synthesis gas; oxy-combustion which separates oxygen from air prior to combustion and produces a nearly sequestration-ready $CO_2$ effluent and post-combustion, $CO_2$ capture from power plant flue gas [8, 9]. This work is focused on post-combustion $CO_2$ capture. Post-combustion carbon capture appears to be the most adequate strategy for integration with existing coal-fired power plants [10]. Flue gases from post-combustion processes typically comprise 10-15% $CO_2$, 90-85% $N_2$ and minor concentrations of other gases [11].

Many methods exist for removing $CO_2$ capture. One such method utilizes absorption in aqueous solutions of alkanolamines using conventional equipment, such as packed columns, bubble columns, and spray columns [12].

In a typical post-combustion capture process, treated flue gas is passed through a chemical absorption column where solvents absorb carbon dioxide. The $CO_2$-rich solvent is then regenerated by heating in a stripper unit. The freed $CO_2$ is then compressed for storage or use [13].

Most post-combustion processes are compatible with existing coal-fired power plant infrastructures without requiring substantial changes to basic combustion technologies. These processes are leading candidates for retrofitting gas-fired power plants and are promising for the development and commercialisation of integrated coal gasification combined cycle (IGCC) in power generation applications [14].

Hollow fibre gas-liquid membrane contactors are alternatives to conventional gas absorption systems for $CO_2$ capture. A membrane contactor combines the advantages of membrane technology with those of an absorption liquid [15]. Hollow fibre membrane contactors could potentially overcome the disadvantages of conventional absorption systems and develop more effective $CO_2$ capture technologies [16]. These membranes are flexible in operation and maintenance, modular, energy efficient, ease of install by skid-mounting, ability to be applied in remote areas (such as offshore) and have high specific surface areas [17]. The absorption process provide very high selectivity and high driving forces for mass transfer even at very low concentrations [18]. The separation of two phases by the membrane leads to the prevention of flooding and foaming of the absorbent liquid [19].

As a means for process intensification, membrane contactors were recently explored by Bounaceur et al. (2012), and Favre (2011) [20, 21]. The application of these contactors include a large number of fields where chemical or physical absorption is the natural separation technology, i.e., natural gas sweetening and dehydration and post and pre-combustion $CO_2$ capture. A rigorous comparison of the effective intensification potential of membrane contactors with packed columns is necessary to more accurately determine the mass transfer intensification factor, which has been reported over a broad range, i.e., from 0.8 to 10 (with MEA for $CO_2$ absorption) [20].

A literature review shows that most studies in this area have focused on the absorption of carbon dioxide by hollow fibre microporous membranes comprising hydrophobic polymers, such as poly(propylene) (PP), poly(ethylene) (PE), poly(tetrafluoroethylene) (PTFE) and poly(vinylidene fluoride) (PVDF) [19].

Poly(vinylidene fluoride) (PVDF) membranes have low surface energy values [22]. Many advantages make this polymer a promising candidate to capture carbon dioxide using hollow fibre membrane contactors. PVDF is a hydrophobic polymer and can be dissolved in common solvents to prepare asymmetric membranes via phase-inversion [23]. Hence it can easily be converted to asymmetric membranes via phase inversion method, resulting in easy controlled membrane structure and morphology [24]. PVDF, which has high fluorine content, is relatively cheap and easily available [25]. Moreover, PVDF fibres have high thermal and chemical resistance along with good mechanical strength [26]. Previous authors, proposed methods to improve the properties of PVDF membranes. One of these methods is the use of a relatively neutral coagulation bath instead of pure water to prevent formation of dense skin layer [24, 27, 28]. The coagulation bath could be formed by water and N,Ndimethylacetamide (DMAc) or N-Methyl-2-pyrrolidone (NMP). DMAc is the most commonly used solvent but NMP satisfies the kinetic criterion coagulation and allows the production of permeable membranes [28]. For this reason, the fabrication parameters during phase-inversion can be controlled to develop appropriate membrane structures for contactor applications [22]. Some previous works supported the use of PVDF membrane contactors in order to capture $CO_2$ [29-31].

Alkanolamines have been traditionally used for carbon dioxide capture due to their low costs and high reactivity with $CO_2$. Alkanolamines are able to form weakly bound complexes with $CO_2$ to produce effluent streams with very low $CO_2$ concentration. However, the regeneration temperature for the $CO_2$-rich solutions is usually higher than 393 K, which would induce thermal degradation and the volatile loss of solvents [32]. Other problems using these solvents are energy consumption for absorbent regeneration, corrosion of industrial equipment materials and foam production [33].

The combination of ionic liquids (ILs) with membrane technology provides new ways to make membrane-based separations a more competitive $CO_2$ separation technology [34]. Many studies have improved $CO_2$ absorption capacities by taking advantage of the tunable properties of ILs [11].

ILs have remarkable properties, such as negligible volatility, high thermal stability, inflammability, tunability, solvation properties, and high $CO_2$ solubility [35]. ILs could potentially replace traditional industrial solvents, which are often volatile organic

compounds (VOCs) [11]. A few ionic liquids have been found to have high solubility capacities for $CO_2$ and $SO_2$ and have been studied as potential absorption liquids [36, 37].

ILs with acetate anions possess high degree of absorption for $CO_2$ across a wide range of temperatures [38]. To achieve a high $CO_2$ absorption efficiency, a liquid with a high $CO_2$ diffusion coefficient and/or a high $CO_2$ solubility is required. For this reason. In this work, 1-ethyl-3-methylimidazolium acetate ([emim][Ac]) ionic liquid was used. This IL is an ideal candidate for $CO_2$ capture due to its high $CO_2$ solubility (8.6%) and physical and chemical absorption [39-42]. Additionally, this ionic liquid has been used in other applications, e.g., as a corrosion inhibitor [43]. Carbon dioxide chemisorption by [emim][Ac] has been demonstrated by previous works using NMR spectroscopy and X-ray diffraction [41, 44]. Gurau et al. (2011) proposed a possible reaction of $CO_2$ with [emim][Ac] [44]. Figure 1 shows the molecular structure of the IL, and a possible reaction mechanism with $CO_2$, and the formation of a corresponding imidazolium carboxylate. [emim][Ac] has been well-characterised in other studies [45-47]. Moreover, Carvalho et al.(2009) suggested a preferencial interaction of the acid carbon of the $CO_2$ molecule with the carboxylate group of the acetate anion [48].

An intense study of self-made PVDF inmobilized with [emim][Ac] hollow fibre membrane contactor using [emim][Ac] were used for the non-dispersive absorption of $CO_2$. PVDF membranes due to its high hydrophobicity could be used with ionic liquids and therefore allows working in non-wetted mode. On other hand, it is worth recalling that this ionic liquid possess a carboxylic anion and therefore is promising for $CO_2$ capture. Moreover, [emim][Ac] has a reversible interaction with $CO_2$. This property is a key factor for the regeneration ability of the IL in its industrial application. The $CO_2$ capture efficiency and mass transfer coefficient $K_{overall}$ were also evaluated. Gas, membrane and liquid resistances were also calculated. The obtained values were compared with those reported in the literature. A numerical analysis was carried out to estimate mass transfer effects. The membrane mass transfer coefficient, membrane dimensions, and module design were evaluated to determine whether a significant intensification effect was observed for a membrane contactor when compared with a conventional packed column. The aim of the numerical analysis performed in this work is to contribute to this objective. Additional work on membrane contactors may focus on optimizing membrane geometry and module design. Future work could develop rigorous

models essential for the successful scale-up and evaluation of membrane contactors in various applications [49].

## 2. Experimental

### *2.1 Hollow fibre membranes*

Poly(vinylidene fluoride) (PVDF) hollow fibre membranes with additives called 1AQ2 fibres were homemade-cast via phase-inversion. The PVDF material was HSV900 grade from Arkema (France). N-methyl-pyrrolidone (NMP) was used as a solvent, and LiCl (Aldrich-France) with a block copolymer were used as additives. The 1AQ2 fibres were composed of 15% PVDF HSV900, 3% block copolymer, 3% LiCl and 1% water [28, 50]. The fibre manufacturing method was explained in detail in previous works [28, 50-53]. The composition of the fibres were water/NMP:70/30% [28]. Additives first are dissolved in the solvent for 24 hours under mechanical stirring in a water bath at 323K by condensing vapors to prevent solvent evaporation. PVDF is then added raising the temperature to 330K to facilitate dissolution. Removing air bubbles trapped in the collodion by putting the primary vacuum to 353K. Collodions then stored at 323K until use. Besides the dimensions and design of the extrusion die, the operator can play during manufacture of flow rates and temperatures of the internal liquid collodion and the composition of the internal fluid, the air gap (distance between the die and the coagulation bath), the humidity in the air, the composition and temperature of the coagulation bath and the spinning speed imposed by the cylinders, ten operating parameters, to modify the properties of the manufactured fibre [28]. After phase-inversion, 150mL of IL was added to the developed membrane in continuous stirring during 48h at room temperature. Finally, the virgin fibres were dried after adding the IL. Subsequently, 1-ethyl-3-methylimidazolium acetate [emim][Ac] was immobilized into the fibres.

During drying, the fibres were maintained for approximately 72 hours in an oven at 323 K and atmospheric pressure.

The membrane contactor was manufactured by gluing hollow fibres in a PVC shell. In the 1AQ2 hollow fibre membrane contactor, 11 fibres were assembled. The main characteristics of the membrane contactors are shown in Table 1.

*2.2 $CO_2$ capture process*

A gas-liquid membrane contactor module was used in order to determine the membrane mass transfer resistance and study the effect of operating parameters on $CO_2$ absorption. The membrane has been checked with pure $CO_2$ from 0 to 14 bar. At these pressures the fibres were stable and the membrane did not suffer degradation. This could imply that the ionic liquid filled the pores, and thus, the gas was unable to enter fibres. This is a good quality for the fibres because the membrane works in non-wetted mode because the pores are completely filled.

The experimental setup is shown in Figure 2. The feed Gas stream contained 15 vol.% $CO_2$ and 85 vol.% $N_2$. The flow gas was adjusted using a mass flow controller (Brooks Instrument MFC 5850, Emerson Process Management, Spain). As can see, there is a rotameter in order to check that the mass flow controllers are calibrated. Feed gas was directed through the inside of the hollow fibres. The gas flow rate varied from 20 to 70 mL $min^{-1}$. 1-Ethyl-3-methylimidazolium acetate flowed in a counter-current direction through the shell side. The IL was pumped from a storage tank. The liquid line (50 mL $min^{-1}$) was maintained by a digital gear pump (Cole Parmer Instrument Company, Hucoa-Erloss S.A, Spain).

The experiments were performed over the temperature range of 303-343 K. Each experiment was replicated three times, and the average value was calculated. To maintain isothermal conditions, the hollow fibre membrane contactor and the liquid line were kept in an oven.

Previous studies have reported that [emim][Ac] can be regenerated without degradation [38, 51]. For this propose, a $N_2$-rich gas stream was directed through the lumen side of the hollow fibre membrane until the analyser indicated that the $CO_2$ concentration was constant and near zero. Previous works have demonstrated that [emim][Ac] exhibited a strong but reversible chemical absorption for $CO_2$ and that [enim][Ac] is similar to other ionic liquids, such as [bmim][Ac], due to the presence of an imidazolium cation and an acetate anion [40, 53]. It was not necessary change the ionic liquid during the whole experimental planning.

The $CO_2$ concentration of the outlet gas stream was continuously monitored by sampling a fraction of the stream using a gas analyser (Emerson Process) based on non-dispersive infrared (NDIR) spectroscopy. Before sending the gas sample to the analyser, the sample was diluted with $N_2$ to maintain a constant concentration range for the NDIR analyser (at least 200 mL $min^{-1}$). A steady state condition was indicated by a constant $CO_2$ concentration in the exit gas stream.

## *3. Results and discussion*

### *3.1. $CO_2$ capture efficiencies with [emim][Ac] in a PVDF membrane module.*

Carbon dioxide absorption experiments with 1-ethyl-3-methylimidazolium acetate were carried out in a PVDF membrane contactor to evaluate the $CO_2$ capture efficiency at different temperatures. The outlet concentration of carbon dioxide at pseudo-steady-state was calculated using equation 1:

$$Efficiency\ (\%) = \left(1 - \frac{C_{CO_2,out}}{C_{CO_2,in}}\right) \cdot 100 \qquad (1)$$

where $C_{CO2,out}$ is the outlet concentration of $CO_2$ and $C_{CO2,in}$ is the inlet concentration of $CO_2$ (15%).

The $CO_2$ removal efficiencies were calculated from the inlet and outlet $CO_2$ concentrations for the absorption experiments (Table 2). The experiments were performed at different temperatures with gas flow rates of 20 mL $min^{-1}$ and 70 mL $min^{-1}$ using a 1AQ2-PVDF membrane contactor. The efficiency increased when the temperature increased, especially from 303 to 313 K. The experimental error in Table 2 is the deviation of the results of at least three replicated experiments. Within this range, there was a sharp drop in viscosity and low solubility losses.

Based on the results, the following observations were made: (i) as the gas flow decreased, higher residence times were recorded in the contactor and the efficiency increased; and (ii) the efficiency also increased when the temperature increased. At a gas flow rate of 20 mL $min^{-1}$, the absorption efficiency was 20.5% at 303 K and 29.3% at 333 K. These values allow the non-dispersive absorption using PVDF membranes and [emim][Ac] ionic liquid be considered as a promising technique for carbon dioxide capture. In

addition, working at 333K, coupled seven modules in series disposition with a gas a flow rate of 20 mL $min^{-1}$ around 90% of $CO_2$ recovery could be reached. On the other hand it is possible to place as many modules in parallel as be necessary for other gas flow rates.

### *3.2 Overall mass transfer parameter of $CO_2$ absorption with [emim][Ac] in a PVDF membrane module.*

In industrial applications, the mass transfer coefficient is a crucial parameter used to estimate the size of a contactor [54]. This parameter is a diffusion rate constant that relates the mass transfer rate, mass transfer area, and concentration change as driving force.

The overall transfer coefficient, $K_{overall}$, can be experimentally determined from the $CO_2$ flux through the membrane. This parameter is calculated using equation 2 (Table 3):

$$N_{CO_2,g} = \frac{Q_g}{A}\left(C_{CO_{2,in}} - C_{CO_{2,out}}\right) = K_{overall}\frac{\Delta ylm \cdot P_T}{RT} \quad (2)$$

where $Q_g$ is the gas flow rate ($m^3\ s^{-1}$), $A$ is the membrane area ($m^2$), $P_T$ is the total pressure in the gas phase, and $\Delta ylm$ is the logarithmic mean of the driving force based on the gas phase molar fractions.

Table 3 shows the values $K_{overall}$ at different gas flow rates using a hollow fibre membrane contactor with 1AQ2 fibres. The temperature was varied from 303 to 343 K. Figure 3 shows the different values obtained at flow rates of 20 and 70 mL $min^{-1}$. The trend was the same as that in the previous section. The differences were greater from 303 to 313 K due to the influence of viscosity and minimal variation in solubility.

### *3.3. A resistance-in-series approach for $CO_2$ absorption with [emim][Ac] in the PVDF membrane module.*

The resistance-in-series approach can be used to correlate individual mass transfer resistances to the overall mass transfer resistance, $K_{overall}$. $K_{overall}$ is given by the summation of the gas, membrane and liquid film resistances, as indicated in equation 3 [36, 51, 55]:

$$R_{overall} = R_g + R_m + R_l \quad (3)$$

The liquid phase and gas phase were directed through a hollow fibre configuration in the shell side and lumen side, respectively. The mass transfer process consisted of three consecutive steps: diffusion of a gaseous component from the bulk gas phase to the outer surface of the membrane, diffusion through membrane pores to the gas–liquid interface and chemical reaction at the gas-liquid interface [56].

$CO_2$ absorption essentially takes place at the gas-liquid interface. The role of liquid hydrodynamic distribution (i.e., solvent velocity profile) can be expected to play a minor role [20].

The resistance in series approach (Equation 3) can also be expressed as Equation 4:

$$\frac{1}{K_{overall}} = \frac{d_0}{k_g\, d_i} + \frac{d_0}{k_{mg}\, d_{lm}} + \frac{1}{k_l\, H_d\, E} \tag{4}$$

where $d_o$, $d_i$ and $d_{lm}$ are the outside, inside and log mean diameters (m) of the hollow fibres; $k_g$, $k_{mg}$, and $k_l$ are the individual mass transfer coefficients of the gas phase, membrane and liquid phase, respectively (m $s^{-1}$); $E$ is the enhancement factor, this factor can quantify the chemical reaction effect [39, 55, 57]; $K_{overall}$ is the overall mass transfer coefficient (m $s^{-1}$) and $H_d$ is the dimensionless Henry constant. $H_d$ was calculated by Eq. 5 using the Henry's law constant ($H_c$) [55]:

$$H_d = H_c RT \tag{5}$$

Finally, $k_l$ was estimated using Kartohardjono´s correlation (Eq. 6) because the packing factor and Reynolds number were within range ($0.029<\varphi<0.53$; $Re<400$) [39]:

$$Sh = \left(\frac{k_l\, d_h}{D_{CO_2,l}}\right) = 0.1789\ (\varphi^{0.86})\ Re^{0.34}\ Sc^{\frac{1}{3}} \tag{6}$$

where $D_{CO2,l}$ is the diffusion coefficient of carbon dioxide in the liquid, L is the fibre length and $d_h$ is the hydraulic diameter.

The gas and membrane phases had resistances of 0.02% and 0.23% of the overall resistance, respectively (Table 4). The liquid phase had the highest resistance to mass transfer at nearly 100% of the overall resistance. This was consistent with the obtained results in previous works [36, 39, 51, 55].

Figure 4 shows the logarithm plot of the different resistances against temperature. As expected, different resistance values of gas, liquid and membrane overlapped for different gas flow rates.

### *3.4. Mass transfer enhanced by the chemical reaction for $CO_2$ absorption with [emim][Ac] in the PVDF membrane module.*

Gurau et al. (2011), reported on the single-crystal X-ray structures of solid-state products obtained from the reaction of $CO_2$ with acetate ILs, which confirm the reaction mechanism: the crystal structure confirmed the formation of imidazolium carboxylate molecules (Figure 1) [44].

In order to contribute to the analysis of the chemical reaction, an approach from the mass transfer results was carried out. The obtained values of $K_{overall}$ were transformed using equation 7 to compare the results from the 1AQ2 hollow fibre module with previously reported values. The transformed constant, $K_r$ ($s^{-1}$) may agreed with a first-order, gas–liquid chemical reaction, indicating the accumulation of $CO_2$ in the liquid media [36].

$$K_r = K_{overall} \frac{fiber\ area}{shell\ volume} \tag{7}$$

The component diffusivities and the reaction rate steadily increased with the temperature. The solubility decreased as the temperature increased. The temperature increased as a response to competing phenomena and had an opposite effect on the reaction rate and solubility. This could lead to a complex absorption behaviour [56].

Table 5 compares the overall rate constant and transformed rate constant of the PVDF hollow fibre membrane contactor with other reports in the literature for different types of solvent [54, 59-65]. The fibre sizes in the 1AQ2 membrane contactor agreed with those of the literature. Mansourizadeh et al., used fibres with similar inner and outer diameters, $7.50 \cdot 10^{-4}$ and $4.20 \cdot 10^{-4}$ m, respectively [60, 61]. Taking into account the number of fibres, several authors used between 5 and 11 [54, 60-64]. However, Rongwong et al. and Wang et al., each used 35 and 150 fibres, respectively [59, 62]. For this reason, the ratios between the fibre area and the shell volume were higher in these cases.

Regarding $K_{overall}$, the obtained values for this study were almost one order of magnitude higher than previous works (Table 5) that used traditional solvents, such as monoethanolamine (MEA), diethylamine (DEA), adenosine monophosphate (AMP) and water. As the different parameters such as outer and inner fibre diameter, module length, number of fibres and the fibre area/shell volume are in concordance with the previous articules, the high overall mass transfer coefficient implies that the transfer carbon dioxide-ionic liquid is more facilitated than with traditional solvents. Moreover, these solvents have been traditionally associated with some operational problems due to volatility and solvent losses. Ionic liquids can be used to eliminate these drawbacks. Therefore it is worth recalling that the ILs have a number of advantages over traditional solvents, such as negligible vapour pressures, high thermal, electrochemical and chemical stability and loss less regenerative abilities [11, 35].

As in the previous sections, different values of $K_r$ were calculated for the different temperatures and flow gas streams (Table 6).

Using the Arrhenius equation and the different values of $K_r$ at different gas flow rates (Table 6), the activation energy was calculated according to equation 8.

$$Kr = B \cdot e^{\frac{-Ea}{R \cdot T}} \quad (8)$$

where $B$ is a pre-exponential factor, $Ea$ is the activation energy (J $mol^{-1}$), $R$ is the gas constant 8.31 (J $K^{-1}$ $mol^{-1}$), and $T$ is the temperature (K). The activation energy for [emim][Ac] in $CO_2$ was 9.2 kJ $mol^{-1}$ with a confidence of $R^2$=0.92.

Table 7 compares the activation energy obtained in the present work with values for different ionic liquids in the literature [66-70]. A few observations can be made: (i) ionic liquids in the presence of other solvents, such as MEA, AMP, aprotic heterocyclic anions (AHA) or water, have higher activation energies than the value obtained herein [65-68]; and (ii) when ILs were not mixed with other solvents, the reported activation energy value agreed with the value calculated in this work. For the same [$P_{66614}$] cation, Burkan et al., reported activation energies of 18 and 11 kJ $mol^{-1}$ for the anions [3-CF3pyra] and [2-CNpyr], respectively [70].

The reported $Ea$ values for conventional solvents, such as amines (which react with $CO_2$), ranged from 40-55 kJ $mol^{-1}$ [70]. These values were significantly higher than the results

obtained in this work using the ionic liquid [emim][Ac]. This phenomenon can be explained by a differences in the coupling mechanisms, interfacial reactions and mass transfer in the liquid phase.

An approach to describe the overall temperature dependence in reactive absorption processes has been applied to hollow fibre membrane contactors by Boucif et al. (2015) [58], based on the Shah criterion [71]. The use of an effective activation energy was proposed in terms of a parameter $\gamma_{eff}$ calculated using the Equation 9.

$$\gamma_{eff} = \frac{1}{2}(\gamma_{Da} + \gamma_R) - \gamma_s \quad (9)$$

where $\gamma$ are dimensionless activation energies, assuming that the solubility, the diffusivity and the reaction rate constant are Arrhenius type dependent on temperature.

$\gamma_{eff}$ explains two different phenomena, on one hand an increase in diffusivity and reaction rate and on the other hand a reduction in solubility for a rise in temperature. Boucif et al., reported the different meanings of $\gamma_{eff}$ as a function of its positive, negative or zero value [58].

The values of $\gamma_{eff}$ obtained in this work for the interaction $CO_2$-[emim][Ac] are slightly upper than zero (0.4). Thus, the increase in reaction rate coefficient and diffusion coefficient with temperature may play dominant role in the overall temperature dependence.

*3.5. Simulation task to estimate mass transfer and operational effects.*

A set of module conditions have been evaluated (i.e., membrane mass transfer coefficient, membrane dimensions, and module design) to determine whether a significant intensification effect was present for a membrane contactor when compared with a packed column.

A long-term, stable operation of the hollow fibre membrane contactor requires that the pores of the membrane remain completely gas-filled over prolonged operational periods. If the membranes are even partially wetted, the overall mass transfer resistance increases because the absorbed gas has to diffuse through stagnant liquid inside the pores. Because aqueous alkanolamine solutions increase the potential for membrane wetting, other

absorption liquids, such as ILs, may offer higher surface tensions and more consistent performance.

The modelling of the transfer of $CO_2$ from the gas phase to the liquid phase through the membrane barrier was simulated using Aspen Custom Modeler software (Aspen Technology, Inc.). Figure 5 shows the coordinates of the fibre. The radial position r=0 is the centre of the fibre, and the axial distance of z=0 indicates the initial position of the gas in the fibre. The differential mass balance on $CO_2$ (eq. 10) was based on the following assumptions: a negligible concentration of the soluble gas in the absorption liquid, steady state and isothermal conditions, no axial diffusion, ideal gas behaviour and constant tube side and shell side pressures [72, 73].

$$u_z \frac{\partial C_{CO_2}}{\partial z} = D\left[\frac{1}{r}\frac{\partial}{\partial r}\left(r\frac{\partial C_{CO_2}}{\partial r}\right)\right] \tag{10}$$

Equation 10 can be transformed assuming the gas velocity is a fully developed laminar flow [72]:

$$2u_m\left[1-\left(\frac{r}{R}\right)^2\right]\frac{\partial C_{CO_2}}{\partial z} = D\left[\frac{1}{r}\frac{\partial}{\partial r}\left(r\frac{\partial C_{CO_2}}{\partial r}\right)\right] \tag{11}$$

Equation 11 can be rewritten in the dimensionless form:

$$\frac{Gz}{2}[1-\bar{r}^2]\frac{\partial \bar{C}_{CO_2}}{\partial \bar{z}} = \frac{1}{\bar{r}}\frac{\partial}{\partial \bar{r}}\left(\bar{r}\frac{\partial \bar{C}_{CO_2}}{\partial \bar{r}}\right) \tag{12}$$

where the dimensionless variables are defined as:

$$\bar{r} = \frac{r}{R} \tag{13.a}$$

$$\bar{z} = \frac{z}{L} \tag{13.b}$$

$$\bar{C}_{CO_2} = \frac{C_{CO_2}}{C_{CO_2,inlet}} \tag{13.c}$$

The boundary conditions used were the following:

$$\bar{r} = 0 \rightarrow \frac{\partial \bar{C}_{CO_2}}{\partial \bar{r}} = 0 \tag{14.a}$$

$$\bar{r} = 1 \rightarrow \frac{\partial \bar{C}_{CO_2}}{\partial \bar{r}} = -\frac{Sh}{2}\,\bar{C}_{CO_2} \qquad (14.b)$$

$$\bar{z} = 0 \rightarrow \bar{C}_{CO_2} = 1 \qquad (14.c)$$

and the dimensionless numbers:

$$Gz = \frac{u_m\, di^2}{D\, L} \qquad (15.a)$$

$$Sh = \frac{K_{overall}\, di}{D} \qquad (15.b)$$

The $CO_2$ concentration at the outlet of the module is calculated as a dimensionless mixing cup:

$$\bar{C}_{CO_2=L} = 4\int_0^1 \bar{C}_{CO_2}\,[1-\bar{r}^2]\bar{r}\,d\bar{r} \qquad (16)$$

The modelling results for a gas flow rate of 20 mL $min^{-1}$ and the parameters specified in Table 1 are shown in Figure 6. The $K_{overall}$ ($1.7\cdot10^{-5}$ m $s^{-1}$) obtained in paragraph 3.2 was used. Figure 6a shows the dimensionless carbon dioxide concentration and the capture efficiency along the dimensionless length at 303 K (corresponding to $K_{overall}$ value of $1.7\cdot10^{-5}$ m $s^{-1}$). Figure 6b shows the simulation results for the temperature interval 303-333 K. These results closely matched the experimental values.

Different radial nodes are shown in these figures from the centre of the fibre (r=0) to the membrane surface layer (r=1). To show the difference between non-wetted and wetted modes, Figures 6a, 6c and 6d were prepared. Different nodes in the radial dimension are provided from the centre of the fibre (r=0) to the membrane surface layer (r=1). In the wetted mode, as the Graetz number is large, the concentration profile in the radial dimension builds up, and a significantly lower efficiency (8%) than that of the non-wetted mode was observed.

A sensitivity analysis was performed to estimate the mass transfer effect on the $CO_2$ capture efficiency operating in non-wetted mode. A 90% efficiency was the design target

[21]. Previous works that reported 90% $CO_2$ capture efficiencies using PVDF membrane contactors used alkanolamines, i.e., primarily MEA [74-77]. The aim of this simulation was to determine the parameters necessary to reach this efficiency using ionic liquids to provide a cleaner process without solvent loss.

Figure 7 shows different capture efficiencies for varying values of the mass transfer coefficient, $K_{overall}$ (baseline, $1.7 \cdot 10^{-5}$ m $s^{-1}$). Values greater than $1.7 \cdot 10^{-4}$m $s^{-1}$ yielded efficiencies above 90% (Figure. 7a). A more detailed analysis was carried out in Figure 7b. Values were analysed varying the Sherwood number using a fixed Graetz number. For Sherwood number values greater than $4.7 \cdot 10^{-3}$ and a fixed Graetz number ($8.0 \cdot 10^{-3}$), at least 90% efficiencies were achieved.

The intensification factor I was also calculated and shown in Figure 7a. The intensification factor reached the value of 4.5 for the target $CO_2$ efficiency of 90% and was calculated as the volumetric absorption capacity of the membrane contactor divided by the average volumetric absorption capacity of a packed column. The reference value of a classical packed column was estimated for 1 mol $CO_2$ $m^{-3}s^{-1}$ using a 30 wt.% MEA solution [20].

Because 1-ethyl-3-methylimidazolium acetate provided higher $K_{overall}$ values than values reported in the literature, the use of ionic liquids is vital to making membrane contactors competitive at the industrial scale.

In the design of a membrane unit module, membrane elements can be coupled in parallel and in series. In this way, the module can be easily adjusted to achieve a desired removal efficiency. In this simulation, the fibre length was also modified to estimate the number of hollow fibre membrane contactors in series necessary to achieve at least a 90% efficiency. Figure 8a shows the influence of the fibre length. Seven membrane contactors in series (a total length of 2 m) was necessary to reach the target capture efficiency. For a constant, dimensionless Sherwood number, the Graetz number was varied (Fig. 8b). Graetz values smaller than $9.5 \cdot 10^{-4}$ allowed for high efficiencies over 90%.

Based on these simulation results, the total fibre length of 2 m of the membrane unit should be considered during scale up. The efficiency of $CO_2$ capture processes based on sets of membrane modules in series or in parallel that can be estimated based on the

desired flue gas flow rate. Furthermore, the footprint size of the contactors could be reduced by more than 65 % if intensification factors are considered [78].

## *4. Conclusions*

The evaluation of carbon dioxide absorption using a poly(vinylidene fluoride) (PVDF)-[emim][Ac] hollow fibre contactor and 1-ethyl-3-methylimidazolium acetate [emim][Ac] absorption ionic liquid was experimentally verified. The results show that approximately 20-30% of carbon dioxide was recovered under a gas flow rate of 20 mL $min^{-1}$ from 303 to 333 K. Gas and membrane resistances were negligible compared with the overall mass transfer resistance. Liquid resistance accounted for essentially all mass transfer resistance in the contactor modules.

The mass transfer coefficients of the PVDF membrane contactors were compared with reported values in the literature. Polymeric membranes are of great interest for this application because of their hydrophobic character, their commercial availability and reasonable price.

$CO_2$ capture using PVDF fibres achieved a $K_{overall}$ higher than values reported in the literature for other PVDF hollow fibre membrane contactors using conventional solvents. For a gas flow rate of 20 mL $min^{-1}$ at 303 K, the mass transfer coefficient was $1.7 \cdot 10^{-5}$ m $s^{-1}$.

Regarding the activation energy calculations, the hollow fibre membrane contactor with ionic liquid solvent had an activation energy of 9.2 kJ $mol^{-1}$. This energy barrier was much smaller than those obtained with conventional solvents reacting with $CO_2$ (such as MDEA at 43-44 kJ $mol^{-1}$). This may be explained by a coupling mechanism of the interfacial reaction between $CO_2$ and [emim][Ac] and the mass transfer in the liquid phase.

A theoretical simulation was carried out. For a target 90% $CO_2$ capture, the simulation revealed that (i) the mass transfer coefficient should be greater than $1.7 \cdot 10^{-4}$ $m \cdot s^{-1}$ or (ii) seven hollow fibre membrane modules in series (total length of 2 m) were necessary, being proposed for the scaling-up a network of modules in series and as many in parallel as the flue gas flow rate increases.

The intensification potential of the membrane contactor compared with a packed column performance with 30 wt.% MEA solution was estimated by the intensification factor, which reached a value of 4.5 for 90% $CO_2$ capture.

*Acknowledgement*

This research was funded by the Spanish Ministry Economy and Competitive (Project CTQ2013-48280-C3-1-R). The authors thank Dr. J.C. Remigy (Laboratoire de Genie Chimique, UPS, Toulouse, France) for the preparation of 1AQ2-PVDF fibres.

*Symbols used*

| | | |
|---|---|---|
| $A$ | [$m^2$] | effective membrane area |
| $B$ | [-] | pre-exponential factor |
| $D$ | [$m^2\ s^{-1}$] | diffusivity |
| $d_h$ | [m] | hydraulic diameter |
| $d_i$ | [m] | inside diameter of the fibre |
| $d_{lm}$ | [-] | log mean diameter of the fibre |
| $d_o$ | [m] | outside diameter of the fibre |
| $E$ | [-] | enhancement factor |
| $Ea$ | [J $mol^{-1}$] | activation energy |
| $Gz$ | [-] | Graetz number |
| $H_d$ | [-] | dimensionless Henry's law constant |
| $H_c$ | [mol $bar^{-1}\ L^{-1}$ ] | Henry's law constant |
| $k_g$ | [m $s^{-1}$] | mass transfer coefficient in the gas phase |
| $k_l$ | [m $s^{-1}$] | mass transfer coefficient in the liquid phase |

| | | |
|---|---|---|
| $k_{mg}$ | [m $s^{-1}$] | mass transfer coefficient of the membrane |
| $K_{overall}$ | [m $s^{-1}$] | overall mass transfer coefficient |
| $L$ | [m] | fibre length |
| $n$ | [-] | number of fibres |
| $N_{CO2}$ | [mol $m^2$ $s^{-1}$] | absorption flux of carbon dioxide |
| $P_T$ | [bar] | total pressure |
| $Q$ | [$m^3$ $s^{-1}$] | flow rate |
| $R$ | [bar L $mol^{-1}$ $K^{-1}$] | ideal gas constant |
| $Re$ | [-] | Reynolds number |
| $R_g$ | [s $m^{-1}$] | resistance in the gas side |
| $R_l$ | [s $m^{-1}$] | resistance in the liquid side |
| $R_m$ | [s $m^{-1}$] | resistance of the membrane |
| $R_{overall}$ | [s $m^{-1}$] | overall resistance to mass transfer |
| $Sc$ | [-] | Schmidt number |
| $Sh$ | [-] | Sherwood number |
| $t$ | [s] | time |
| $T$ | [K] | temperature |
| $u_m$ | [m $s^{-1}$] | linear velocity |

Subscripts

g gas

l liquid

in inlet of the contactor

out outlet of the contactor

Greek letters

| | | |
|---|---|---|
| φ | [-] | packing factor |
| γ | [-] | dimensionless activation energy |

*References*


[1] K. Wang, X. Wang, P. Zhao, X. Guo, *Chem. Eng. Technol*. **2014**, 37(9), 1552–1558. DOI: 10.1002/ceat.201300584.

[2] B. Zhu, Q. Liu, Q. Zhou, J. Yang, J. Ding, J. Wen, *Chem. Eng. Technol*. **2014**, 37(4), 635–642. DOI: 10.1002/ceat.201300240.

[3] S. Khaisri, D. de Montigny, P. Tontiwachwuthikul, R. Jiraratananon, *Energy Procedia* **2011**, 4, 688-692. DOI: 10.1016/j.egypro.2011.01.106.

[4] I. Merino-García, E. Álvarez-Guerra, J. Albo, A. Irabien, *Chem. Eng. J*. **2016**, 305, 104-120. DOI: 10.1016/j.cej.2016.05.032.

[5] S. Zhao, P.H.M. Feron, L. Deng, E. Favre, E. Chabanon, S. Yan, J. Hou, V. Chen, H. Qi, *J. Membr. Sci*, **2016**, 511, 180–206. DOI: 10.1016/j.memsci.2016.03.051.

[6] P. Luis P., T. Van Gerven, B. Van Der Bruggen, *Prog. Energy Combust. Sci*. **2012**, 38, 419-448. DOI: 10.1016/j.pecs.2012.01.004.

[7] S. Roussanaly, R. Anantharaman, K. Lindqvist, H. Zhai, E. Rubin, *J. Mebr. Sci*. **2016**, 511, 250-264. DOI: 10.1016/j.memsci.2016.03.035.

[8] M. Kanniche, R. Gros-Bonnivard, P. Jaud, J. Valle-Marcos, J. Amann, C. Bouallou, *Appl. Therm. Eng*. **2010**, 30, 53-62. DOI: 10.1016/j.applthermaleng.2009.05.005.

[9] T.C. Merkel, H. Lin, X. Wei, R. Baker, Power plant post-combustion carbon dioxide capture: An opportunity for membranes. *J. Membr. Sci*. **2010**, 359(1-2), 126-139. DOI: 0.1016/j.memsci.2009.10.041.

[10] A. Fernandez-Barquin, C. Casado-Coterillo, M. Palomino, S. Valencia, A. Irabien, Chem. Eng. Technol. **2015**, 38(4), 658–666. DOI: 10.1002/ceat.201400641.

[11] M. Ramdin, T.W. Loos, T.J.H. Vlugt, Ind. Eng. Chem. Res. **2012**, 51, 8149-8177. DOI: 10.1021/ie3003705.

[12] S. Khaisri, D. de Montigny, P. Tontiwachwuthikul, R. Jiraratananon, *J. Membr. Sci*. **2011**, 376, 110-118. DOI: 10.1016/j.memsci.2011.04.005.

[13] B. Singh, A.H. Strømman, E.G. Hertwich, *Int. J. Greenh. Gas Control* **2011**, 5, 911–921. DOI: 10.1016/j.ijggc.2011.03.012.

[14] H. Herzog, J. Meldon, A. Hatton, *Advanced Post-Combustion $CO_2$ Capture*. Massachusetts Institute of Technology: Cambridge, MA **2009**.

[15] K. Simons, K. Nijmeijer, M. Wessling, *J. Membr. Sci*. **2009**, 340, 214–220. DOI: 10.1016/j.memsci.2009.05.035.

[16] S.P. Yan, M.X. Fang, W.F. Zhang, S.Y. Wang, Z.K. Xu, Z.Y. Luo, K.F. Cen, *Fuel Process. Technol*. **2007**, 88, 501–511. DOI: 10.1016/j.fuproc.2006.12.007.

[17] R. Khalilpour, K. Mumford, H. Zhai, A. Abbas, G. Stevens, E.S. Rubin, *J. Clean. Prod*. **2015**, 103, 286-300. DOI: 10.1016/j.jclepro.2014.10.050.

[18] A. Mansourizadeh, A.F. Ismail, T. Matsuura, *J. Membr. Sci*. **2010**, 353, 192–200. DOI: 10.1016/j.memsci.2010.02.054.

[19] A. Trusov, S. Legkov, L. Van den Broeke, E. Goetheer, V. Khotimsky, A. Volkov, *J. Membr. Sci*. **2011**, 383, 241– 249. DOI: 10.1016/j.memsci.2011.08.058.

[20] R. Bounaceur, C. Castel, S. Rode, D. Roizard, E. Favre, *Chem. Eng. Res. Des*. **2012**, 90, 2325-2337. DOI: 10.1016/j.cherd.2012.05.004.

[21] E. Favre, *Chem. Eng. J*. **2011**. 171, 782-793. DOI: 10.1016/j.cej.2011.01.010.

[22] A. Mansourizadeh, A.R. Pouranfard, *Chem. Eng. Res. Des*. **2014**, 92, 181-190. DOI: 10.1016/j.cherd.2013.06.028.

[23] M. Rezaei, A.F. Ismail, S.A. Hashemifard, T. Matsuura, *Chem. Eng. Res. D*es. **2014**, 92, 2449-2460. DOI: 10.1016/j.cherd.2014.02.019.

[24] M. Rezaei, A.F. Ismail, Gh. Bakeri, S.A. Hashemifard, T. Matsuura, *Chem. Eng. J*. **2015**, 260, 875-8885. DOI: 10.1016/j.cej.2014.09.027.

[25] Gh. Bakeri, A.F. Ismail, T. Matsuura, M.S. Abdullah, B.C. Ng, M. Mashkour, *Chem. Eng. Res..Des*. 2015, 104, 367-375. DOI: 10.1016/j.cherd.2015.08.024.

[26] H. Fashandi, A. Ghodsi, R. Saghafi, M. Zarrebini, *Int. J. Greenh. Gas Control*. **2016**, 52, 13-23. DOI: 10.1016/j.ijggc.2016.06.010.

[27] M. Peng, H. Li, L. Wu, Q. Zheng, Y. Chen, W. Gu, *J. Appl. Polym. Sci*. **2005**, 98, 1358-1363. DOI: 10.1002/app.22303.

[28] T. Savart, *PhD thesis*, Université Paul Sabatier, Toulouse France **2013**.

[29] A. Mansourizadeh, *Chem. Eng. Res. Des*. **2012**, 90, 555–562. DOI:10.1016/j.cherd.2011.08.017.

[30] H.Y. Zhang, R. Wang, D.T. Liang, J.H. Tay, *J. Membr. Sci*. **2008**, 308, 162-170. DOI: 10.1016/j.memsci.2007.09.050.

[31] S.H. Lin, P.C. Chiang, C.F. Hsieh, M.H. Li, K.L. Tung, *J. Chin. Inst. Chem. Eng*. **2008**, 39, 13–21. DOI: 10.1016/j.jcice.2007.11.010.

[32] M. Fang, Z. Wang, S. Yan, Q. Cen, Z. Luo, *Int. J. Greenh. Gas Control* **2012**, 9, 507-521. DOI: M. Fang, Z. Wang, S. Yan, Q. Cen, Z. Luo, Int. J. Greenh. Gas Control 2012, 9, 507-521.

[33] A.B. López, M.D. La Rubia, J.M. Navaza, R. Pacheco, D. Gómez-Díaz, *Chem. Eng. Technol*. **2014**, 37(3), 419–426. DOI:

[34] Z. Dai, R.D. Noble, D.L. Gin, X. Zhang, L. Deng, *J. Membr. Sci*. **2016**, 497, 1-20. DOI: 10.1016/j.memsci.2015.08.060. [35] J.E. Bara, T.K. Carlisle, C.J. Gabriel, D. Camper, A. Finotello, D.L. Gin, R.D. Noble, *Ind. Eng. Chem. Res*. **2009**, 48, 2739–2751. DOI: 10.1021/ie8016237.

[36] P. Luis, A. Garea, A. Irabien, *J. Membr. Sci*. **2009**, 330, 80–89. DOI: 0.1016/j.memsci.2008.12.046.

[37] J. Albo, P. Luis, A. Irabien, *Ind. Eng. Chem. Res*. **2010**, 49, 11045-11051. DOI: 10.1021/ie1014266.

[38] J. Albo, T. Tsuru, *Ind. Eng. Chem. Res*. **2014**, 53, 8045-8056. DOI: 10.1021/ie500126x.

[39] L. Gomez-Coma, A. Garea, A. Irabien, *Sep. Purif. Technol*. **2014**, 132, 120–125. DOI: 1 0.1016/j.seppur.2014.05.012.

[40] M.B. Shiflett, A. Yokozeki, *J. Chem. Eng. Data* **2009**, 54, 108-114. DOI: 10.1021/je800701j.

[41] X.L. Papatryfon, N.S. Heliopoulos, I.S., Molchan, L.F. Zubeir, N.D. Bezemer, M.K. Arfanis, A.G. Kontos, V. Likodimos, B. Iliev, G.E. Romanos, P. Falaras, K. Stamatakis, K.G. Beltsios, M.C. Kroon, G.E. Thompson, J. Klöckner, T.J.S. Schubert, *Ind. Eng. Chem. Res*. **2014**, 53(30), 12083-12102. DOI: 10.1021/ie501897d.

[42] M.S. Shannon, J.E. Bara, *Ind. Eng. Chem. Res*. **2011**, 50(14), 8665-8677. DOI: 10.1021/ie200259h

[43] M. Hasib-ur-Rahman, F. Larachi, *Ind. Eng. Chem. Res*. **2013**, 52(49), 17682-17685. DOI:

[44] G. Gurau, H. Rodríguez, S.P. Kelley, P. Janiczek, R.S. Kalb, R.D. Rogers, *Angew. Chem. Int. Edit*. **2011**, 50, 12024-12026. DOI: 10.1002/anie.201105198.

[45] A. Yokozeki, M.B. Shiflett, C.P. Junk, L.M. Grieco, T. Foo, *J. Phys. Chem. B*. **2008**, 112, 16654–16663. DOI: 10.1021/jp805784u

[46] M.G. Freire, A.R.R. Teles, M.A.A. Rocha, B. Schroder, C.M.S.S. Neves, P.J. Carvalho, D.V. Evtuguin, L.M.N.B.F. Santos, J.A.P. Coutinho, *J. Chem. Eng. Data***2011**, 56(12), 4813-4822. DOI: 10.1021/je200790q.

[47] W. Shi, C.R. Myers, D.R. Luebke, J.A. Steckel, J.A., D.C. Sorescu, *J. Phys. Chem. B*. **2012**, 116, 283–295. DOI: 10.1021/jp205830d.

[48] P.J. Carvalho, V.H. Alvarez, B. Schröder, A.M. Gil, I.M. Marrucho, M. Aznar, L. Santos, J.A.P. Coutinho, *J. Phys. Chem. B*. **2009**, 113, 6803-6812. DOI: 10.1021/jp901275b.

[49] K.A. Hoff, H.F. Svendsen, *Chem. Eng. Sci*. **2014**, 116, 331-341. DOI: doi.org/10.1016/j.ces.2014.05.001.

[50] O. Lorain, J.M. Espenan, J.C. Remigy, J.F. Lahitte, J.C. Rouch, T. Savart, P. Gerard, S. Magnet, *France* WO2014/139977 (A1) **2014**.

[451] L. Gomez-Coma, A. Garea, J.C. Rouch, T. Savart, J.F. Lahitte, J.C. Remigy, A. Irabien, *J. Membr. Sci*. **2016** 498, 218-226. DOI: 10.1016/j.memsci.2015.10.023.

[52] Y. Medina-Gonzalez, E. Lasseuguette, J.C. Rouch, J.C. Remigy, *Sep. Sci. Technol*. **2012**, 47(11),1596-1605. DOI: 10.1080/01496395.2012.658942.

[53] M.B. Shiflett, D.J. Kasprzak, C.P. Junk, A. Yokozeki, *J. Chem. Thermodyn*. **2008**, 40, 25–31. DOI: 10.1016/j.jct.2007.06.003.

[54] R. Naim, A.F. Ismail, *Sep. Purif. Technol*. **2013**, 115, 152-157. DOI: 10.1016/j.seppur.2013.04.045.

[55] A. Ortiz, D. Gorri, A. Irabien, I. Ortiz, *J. Membr. Sci*. **2010**, 360, 130-141. DOI: 10.1016/j.memsci.2010.05.013.

[56] J.G. Lu, Y.F. Zheng, M.D. Cheng, L.J. Wang, *J. Membr. Sci*. **2007**, 289, 138-149. DOI: 10.1016/j.memsci.2006.11.042.

[57] P. Luis, B. Van der Bruggen, *Greenhouse Gas Sci. Technol*. **2013**, 3, 1–20. DOI: 10.1002/ghg.1365.

[58] N. Boucif, D. Roizard, J.P. Corriou, E. Favre, *Sep. Purif. Technol*. **2015**, 50, 1331-1343. DOI: 10.1080/01496395.2014.969807.

[59] W. Rongwong, R. Jiraratananon, S. Atchariyawut, *Sep. Purif. Technol*. **2009**, 69, 118-125. DOI: 10.1016/j.seppur.2009.07.009.

[60] A. Mansourizadeh, A.F. Ismail, *Chem. Eng. J*. **2010**, 165, 980-988. DOI: 10.1016/j.cej.2010.10.034.

[61] A. Mansourizadeh, A.F. Ismail, Int. *J. Greenh. Gas Control* **2011**, 5, 374-380. DOI: 10.1016/j.ijggc.2010.09.007.

[62] L. Wang, Z. Zhang, B. Zhao, H. Zhang, X. Lu, Q. Yang, *Sep. Purif. Technol*. **2009**, 116, 300-306. DOI: 10.1016/j.seppur.2013.05.051.

[63] M. Rahbari-Sisakht, A.F. Ismail, D. Rana, T. Matsuura, D. Emadzadeh, *Sep. Purif. Technol*. **2013**, 116, 67-72. DOI: 10.1016/j.seppur.2013.05.008.

[64] S. Boributh, R. Jiraratananon, K. Li, *J. Membr. Sci*. **2013**, 429, 459-472. DOI: 10.1016/j.memsci.2012.11.074.

[65] F. Korminouri, M. Rahbari-Sisakht, D. Rana, T. Matsuura, A.F. Ismail, *Sep. Purif. Technol*. **2014**, 132, 601-609. DOI: 10.1016/j.seppur.2014.06.017.

[66] G. Wang, W. Hou, F. Xiao, J. Geng, Y. Wu, Z. Zhang, *J. Chem. Eng. Data* **2011**, 56, 1125-1133. DOI: 10.1021/je101014q.

[67] A. Ahmady, A. Hashim, M.K Aroua, *Chem. Eng. J*. **2012**, 200-202, 317-328. DOI: 10.1016/j.cej.2012.06.037.

[68] Z. Zhou, G. Jing, L. Zhou, *Chem. Eng. J.* **2012**, 204-206, 235-243. DOI: 10.1016/j.cej.2012.07.108

[69] X. Zhang, D. Bao, Y. Huang, H. Dong, X. Zhang, S. Zhang, *AIChE J*. **2014**, 60, 2929-2939. DOI: 10.1002/aic.14507.

[70] B.E. Gurkan, T.R. Gohndrone, M.J. McCready, J.F. Brennecke, *Chem. Chem. Phys*. **2013**, 15, 7796-7811. DOI: 10.1039/c3cp51289d.

[71] Y.T. Shah, *Chem. Eng. Sci*. **1972**, 27, 1469-1474. DOI: 10.1016/0009-2509(72)85033-4.

[72] P. Luis, I. Ortiz, R. Aldaco, A. Garea, A. Irabien, *Int. J. Chem. React. Eng*. **2007**, 5, 1-9.

[73] P. Luis, A. Garea, A. Irabien, *Sep. Purif. Technol*. **2010**, 72, 174–179. DOI: 10.1016/j.seppur.2010.02.003.

[74] S.H. Yeon, K.S. Lee, B. Sea, Y.I. Park, K.H. Le, *J. Membr. Sci*. **2005**, 257, 156–160. DOI: 10.1016/j.memsci.2004.08.037.

[75] S. Paul, A.K. Ghoshal, B. Mandal, *Ind. Eng. Chem. Res*. **2007**, 46, 2576-2588. DOI: 10.1021/ie061476f.

[76] H.Y. Zhang, R. Wang, D.T. Liang, J.H. Tay, *J. Membr. Sci*. **2008**, 308, 162-170. DOI: 10.1016/j.memsci.2007.09.050.

[77] L. Wang, Z. Zhang, B. Zhao, H. Zhang, X. Lu, Q. Yang, *Sep. Purif. Technol*. **2013**, 116, 300-306. DOI: 10.1016/j.seppur.2013.05.051.

[78] K.A. Hoff, H.F. Svendsen *Energy Procedia* **2013**, 37, 952-960. DOI: 10.1016/j.egypro.2013.05.190.

**Figure captions**

Figure 1. Proposed reaction of $CO_2$-[emim][Ac] [44].

Figure 2. Experimental setup for $CO_2$ gas capture.

Figure 3. Representation of $K_{overall}$ values versus temperature.

Figure 4. Log Rx Vs Temperature.

Figure 5. Coordinates of the fibre.

Figure 6. Modelling results for non-wetted mode: (6a) profiles of dimensionless $CO_2$ concentration and process efficiency (%) along the fibre length; (6b) experimental Vs. modelling results at different temperatures. Modelling results for wetted mode: (6c, 6d).

Figure 7. Sensitivity analysis of mass transfer coefficient, K (7a), and the corresponding Sherwood number (7b).

Figure 8. Sensitivity analysis of length module, L (8a), and the corresponding Graetz number (8b). $K_{overall}$ obtained at 333K ($2.5 \cdot 10^{-5}$ m $s^{-1}$) was used as reference value.

**Table captions**

Table 1. Hollow fibre membrane contactor characteristics.

Table 2. Experimental $CO_2$ absorption efficiency.

Table 3. $K_{overall}$ values of $CO_2$ absorption with [emim][ac] in a PVDF hollow fibre membrane modules.

Table 4. Contributions to mass transfer. $CO_2$ absorption with [emim][Ac] in a PVDF membrane module.

Table 5. Fibre size, $K_{overall}$ (m $s^{-1}$) and $K_r$ ($s^{-1}$) comparison with literature values in PVDF hollow fibre membrane contactors.

Table 6. Interfacial rate constant versus temperature, $CO_2$+[emim][ac], PVDF hollow fibre contactor.

Table 7. Activation energy comparison with literature values.

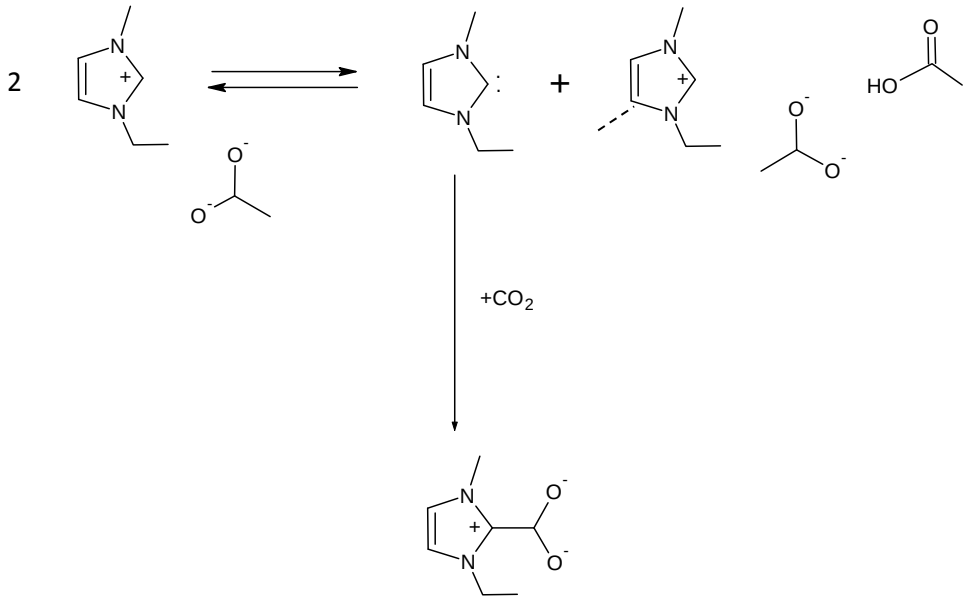


Figure 1.

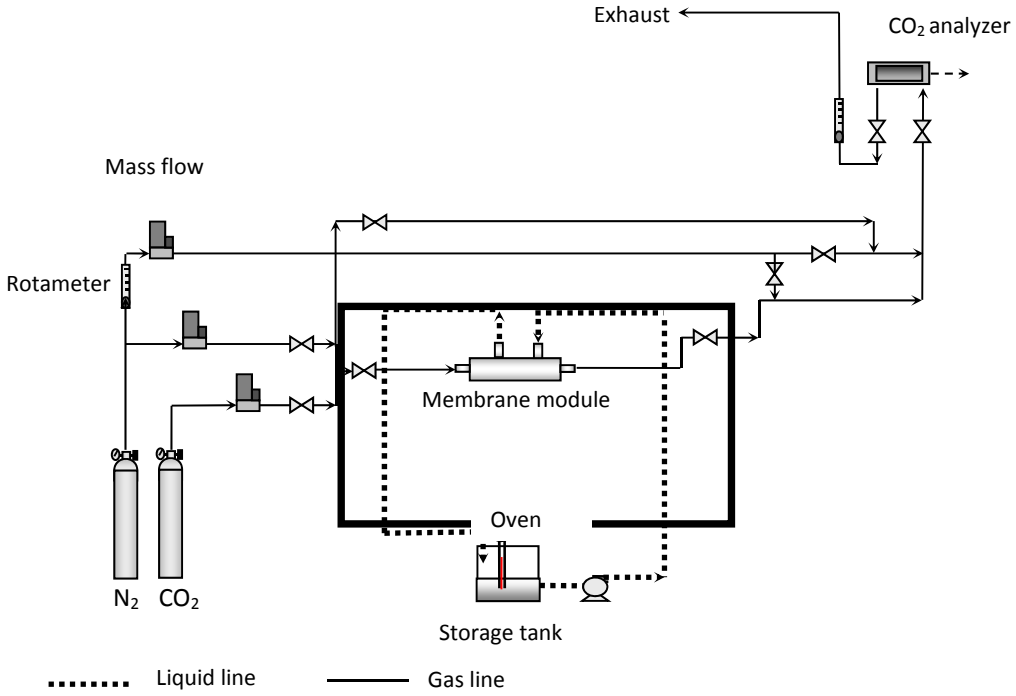
Exhaust
$CO_2$ analyzer
Mass flow
Rotameter
Membrane module
Oven
$N_2$
$CO_2$
Storage tank
Liquid line
Gas line

Figure 2.

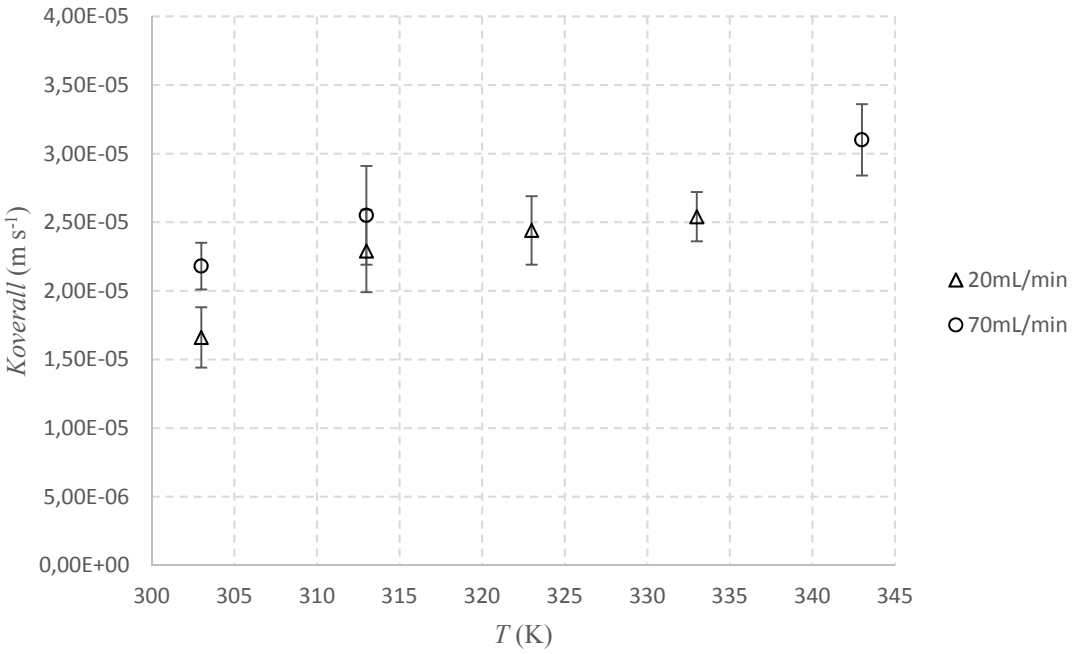
4,00E-05
3,50E-05
3,00E-05
2,50E-05
2,00E-05
1,50E-05
1,00E-05
5,00E-06
0,00E+00
Koverall (m s-1)
300
305
310
315
320
325
330
335
340
345
T (K)
20mL/min
70mL/min

Figure 3.

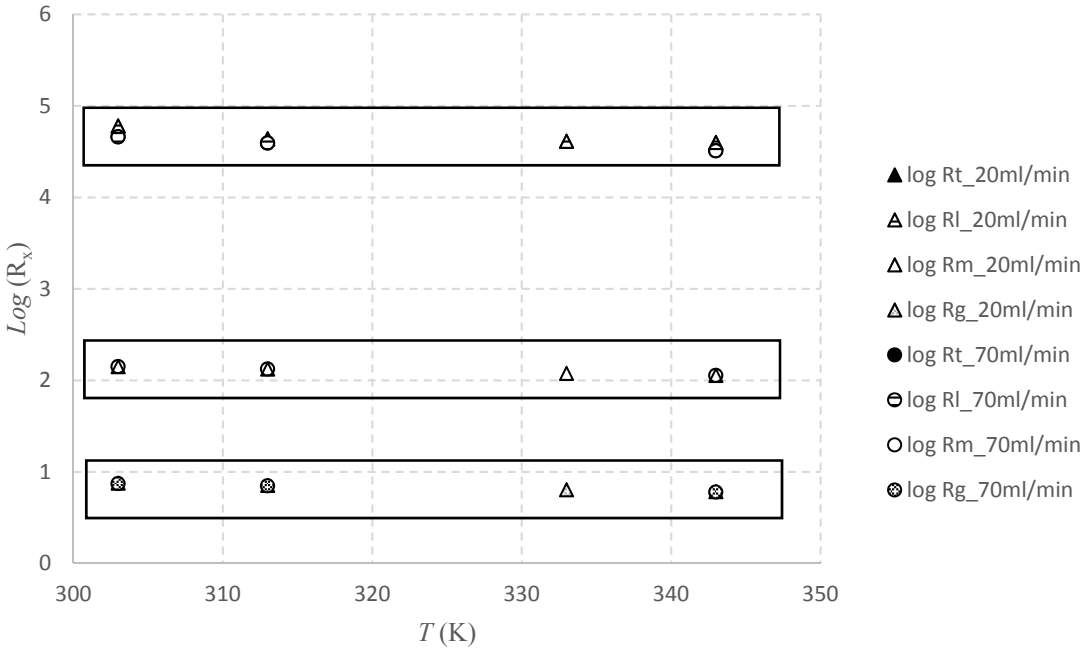
6
5
4
3
2
1
0
Log (Rx)
300
310
320
330
340
350
T (K)
log Rt_20ml/min
log Rl_20ml/min
log Rm_20ml/min
log Rg_20ml/min
log Rt_70ml/min
log Rl_70ml/min
log Rm_70ml/min
log Rg_70ml/min

Figure 4.

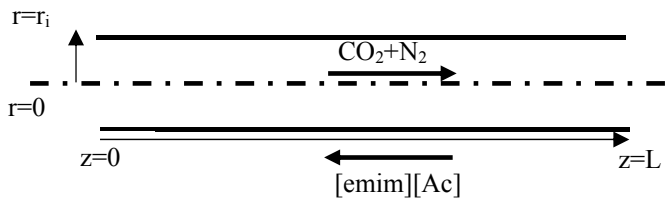


Figure 5.

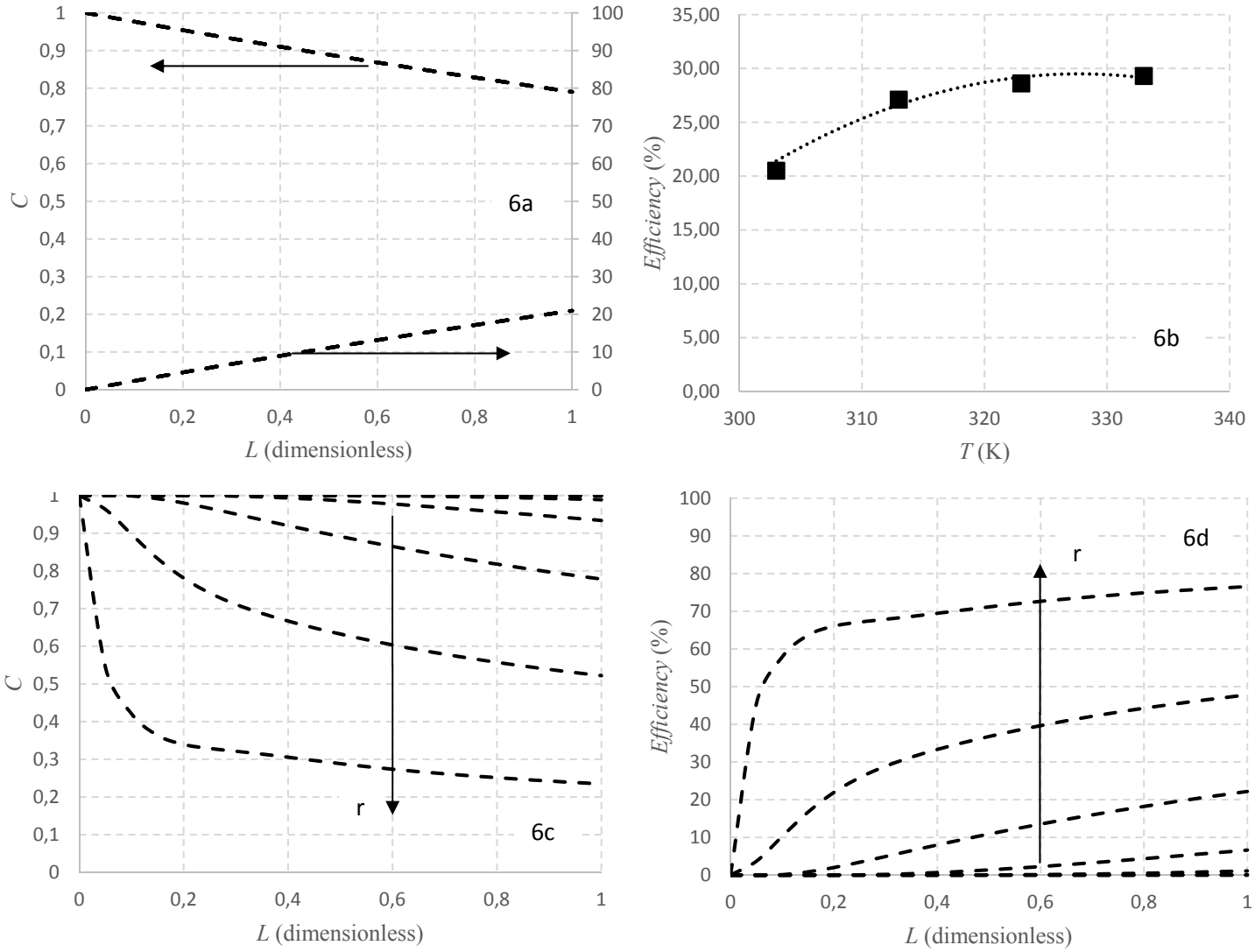


Figure 6.

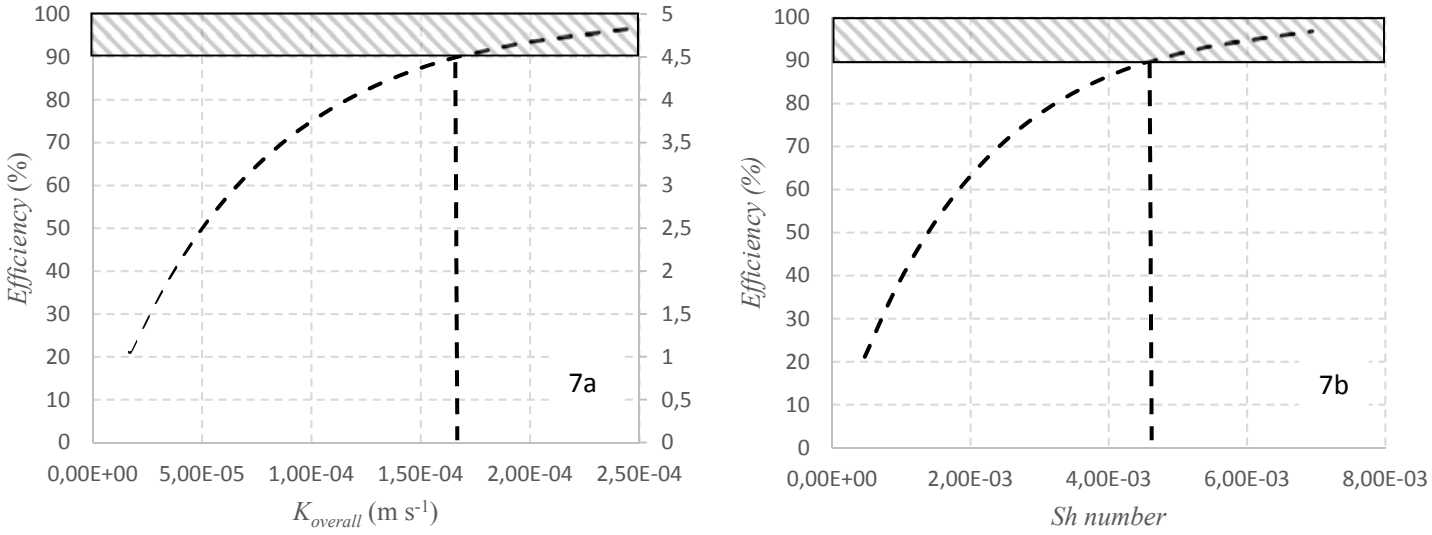
100
90
80
70
60
50
40
30
20
10
0
5
4,5
4
3,5
3
2,5
2
1,5
1
0,5
0
Efficiency (%)
0,00E+00
5,00E-05
1,00E-04
1,50E-04
2,00E-04
2,50E-04
$K_{overall}$ (m $s^{-1}$)
7a
0,00E+00
2,00E-03
4,00E-03
6,00E-03
8,00E-03
Sh number
7b

Figure 7.

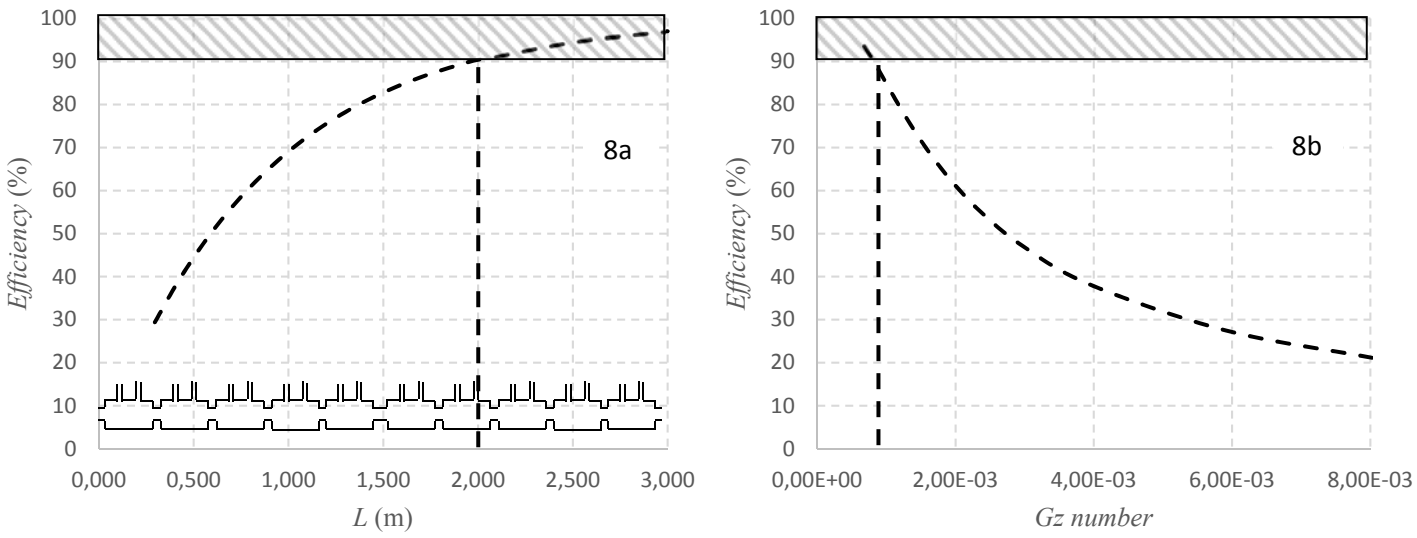
100
90
80
70
60
50
40
30
20
10
0
Efficiency (%)
8a
0,000
0,500
1,000
1,500
2,000
2,500
3,000
L (m)
100
90
80
70
60
50
40
30
20
10
0
Efficiency (%)
8b
0,00E+00
2,00E-03
4,00E-03
6,00E-03
8,00E-03
Gz number

Figure 8.

Table 1.

| | |
|---|---|
| Membrane material | 1AQ2-PVDF |
| Fibre o.d. $d_0$, (m) | $7.7 \cdot 10^{-4}$ |
| Fibre i.d. $d_i$, (m) | $4.51 \cdot 10^{-4}$ |
| Fibre length, $L$ (m) | 0.295 |
| Number of fibres, $n$ | 11 |
| Effective inner membrane area, $A$ ($m^2$) | $4.60 \cdot 10^{-3}$ |
| Porosity (%) | 30 |
| Packing factor | 0.04 |
| Tortuosity[a] | 3.33 |

a Assumed 1/Porosity

Table 2.

| Qg (mL $min^{-1}$) | T (K) | Efficiency (%) |
|---|---|---|
| 20 | 303 | 20.5±2.27 |
| | 313 | 27.1±3.01 |
| | 323 | 28.6±2.51 |
| | 333 | 29.3±1.83 |
| 70 | 303 | 8.2±0.18 |
| | 313 | 9.6±0.35 |
| | 343 | 11.5±0.26 |

Table 3.

| $Q_g$(mL $min^{-1}$) | T(K) | $K_{overall} \cdot 10^5$(m $s^{-1}$) |
|---|---|---|
| 20 | 303 | 1.7±0.2 |
| | 313 | 2.3±0.3 |
| | 323 | 2.4±0.3 |
| | 333 | 2.5±0.2 |
| 70 | 303 | 2.2±0.2 |
| | 313 | 2.6±0.4 |
| | 343 | 3.1±0.3 |

Table 4.

| Qg(mL $min^{-1}$) | T (K) | Rtotal·$10^{-4}$ (s $m^{-1}$) | Rg (s $m^{-1}$) | Rm·$10^{-2}$ (s $m^{-1}$) | Rl·$10^{-4}$ (s $m^{-1}$) |
|---|---|---|---|---|---|
| 20 | 303 | 6.02 | 7.5 | 1.4 | 6.0 |
| | 313 | 4.37 | 7.1 | 1.3 | 4.4 |
| | 323 | 4.10 | 6.4 | 1.2 | 4.1 |
| | 333 | 3.98 | 6.0 | 1.1 | 4.0 |
| 70 | 303 | 4.59 | 7.4 | 1.4 | 4.6 |
| | 313 | 3.92 | 7.0 | 1.3 | 3.9 |
| | 343 | 3.23 | 6.0 | 1.1 | 3.2 |

Table 5.

| Reference | Fibre o.d., m | Fibre i.d., m | Fibre length, m | Module length, m | Module diameter, m | Number of fibres, n | Fibre Area/Shell volume, $m^2 \cdot m^{-3}$ | Solvent | $K_{overall} \cdot 10^5 (m\ s^{-1})$ | $K_r \cdot 10^3 (s^{-1})$ |
|---|---|---|---|---|---|---|---|---|---|---|
| This work | $7.70 \cdot 10^{-4}$ | $4.51 \cdot 10^{-4}$ | $2.95 \cdot 10^{-1}$ | $2.95 \cdot 10^{-1}$ | $1.30 \cdot 10^{-2}$ | 11 | 122 | IL [emim][ac] | 1.70 | 2.00 |
| [41] | $8.00 \cdot 10^{-4}$ | $5.50 \cdot 10^{-4}$ | $2.10 \cdot 10^{-1}$ | $2.50 \cdot 10^{-1}$ | $1.50 \cdot 10^{-2}$ | 10 | 84 | Distilled water | 1.26 | 1.06 |
| [46] | $1.30 \cdot 10^{-3}$ | $8.00 \cdot 10^{-4}$ | $2.95 \cdot 10^{-1}$ | $2.95 \cdot 10^{-1}$ | $1.00 \cdot 10^{-2}$ | 35 | 2742 | 1M MEA | 0.08 | 2.06 |
| | | | | | | | | 1M AMP | 0.04 | 1.10 |
| | | | | | | | | 1M DEA | 0.03 | 0.82 |
| | | | | | | | | Pure water | 0.01 | 0.27 |
| [47] | $7.50 \cdot 10^{-4}$ | $4.20 \cdot 10^{-4}$ | $1.50 \cdot 10^{-1}$ | $2.70 \cdot 10^{-1}$ | $1.40 \cdot 10^{-2}$ | 10 | 48 | Distilled water | 0.25 | 0.12 |
| [48] | $7.50 \cdot 10^{-4}$ | $4.20 \cdot 10^{-4}$ | $1.50 \cdot 10^{-1}$ | $2.70 \cdot 10^{-1}$ | $1.40 \cdot 10^{-2}$ | 10 | 48 | Distilled water | 0.43 | 0.21 |
| [49] | $1.10 \cdot 10^{-3}$ | $8.00 \cdot 10^{-4}$ | $2.40 \cdot 10^{-1}$ | $2.40 \cdot 10^{-1}$ | $4.00 \cdot 10^{-2}$ | 150 | 338 | 1M MEA | 0.09 | 0.32 |
| [50] | $8.50 \cdot 10^{-4}$ | $4.75 \cdot 10^{-4}$ | $1.50 \cdot 10^{-1}$ | $2.70 \cdot 10^{-1}$ | $1.40 \cdot 10^{-2}$ | 10 | 55 | Distilled water | 0.49 | 0.27 |
| [51] | $1.27 \cdot 10^{-3}$ | $7.52 \cdot 10^{-4}$ | $4.50 \cdot 10^{-1}$ | $4.50 \cdot 10^{-1}$ | $8.05 \cdot 10^{-3}$ | 5 | 265 | MEA | 0.33 | 0.88 |
| [52] | $8.09 \cdot 10^{-4}$ | $4.54 \cdot 10^{-4}$ | $2.70 \cdot 10^{-1}$ | $1.75 \cdot 10^{-1}$ | $1.40 \cdot 10^{-2}$ | 7 | 104 | Distilled water | 0.32 | 0.33 |

Table 6.

| Qg(mL $min^{-1}$) | T(K) | $K_r \cdot 10^3$ ($s^{-1}$) |
|---|---|---|
| 20 | 303 | 2.0 |
| | 313 | 2.8 |
| | 323 | 3.0 |
| | 333 | 3.1 |
| 70 | 303 | 2.7 |
| | 313 | 3.1 |
| | 343 | 3.8 |

Table 7.

| Reference | Liquid | Ea kJ $mol^{-1}$ |
|---|---|---|
| This work | [emim][ac] | 9.2 |
| [53] | $[n_{2224}][CH_3COO]$-$nH_2O$ | 21.1 |
| [54] | 4mol·$L^{-1}$ MDEA | 43.32 |
| [54] | 4mol·$L^{-1}$ MDEA+2mol·$L^{-1}$[Bmim][$BF_4$] | 8.65 |
| [55] | $[N_{1111}]$[Gly] + AMP | 40.7 |
| [56] | 30%MEA+65%[Bmim][$NO_3$]+5%$H_2O$ | 77.11 |
| [56] | 30%MEA+60%[Bmim][$NO_3$]+10%$H_2O$ | 63.69 |
| [57] | $[P_{66614}]$[3-CF3pyra] | 18 |
| [57] | $[P_{66614}]$[2-CNpyr] | 11 |
| [57] | $[P_{66614}]$[Pro]+(AHA) | 43 |
| [57] | $[N_{1111}]$[Gly] | 15.4 |
| [57] | 2-((2-Aminoethyl)amino)-ethanol | 32.5 |